JFAChE
Journal of Fundamentals and Applications of Chemical Engineering

Article

iptek.its.ac.id/index.php/ekstrak

Synthesis and Characterization Magnetic Activated Carbon Derived from Coconut Shell for Pb(II) and Cd(II) Adsorption from Wastewater

Armanizar Adji Gumilang[1], Sri Rachmania Juliastuti[2]*

Received Month Day, Year; Revised Month Day, Year; Accepted Month Day, Year
DOI:

Abstract— Activated carbon derived from coconut shell is a low cost adsorbent for heavy-metal removal. However, recovery of spent carbon from treated water remains challenging. This study developed a magnetically separable activated carbon magnetite composite (M-CSAC) and evaluated its adsorption toward Pb(II) and Cd(II). Coconut shell activated carbon (CSAC) was produced by Na_2CO_3 chemical activation and modified by mechanochemical incorporation of Fe_3O_4 through ball milling. SEM–EDX confirmed morphology refinement and successful Fe loading (11 wt.%), while increased surface oxygen indicated Fe–O-rich domains. N_2 adsorption–desorption showed that the specific surface area decreased from 356.04 m^2/g to 319.35 m^2/g. In contrast, total pore volume increased from 0.256 cm^3/g to 0.3166 cm^3/g and the average pore diameter widened from 2.88 nm to 3.97 nm, consistent with mesopore development. XRD reflections at 2θ = 30.24°, 35.40°, 43.18°, 57.00°, and 62.50° matched magnetite (Fe_3O_4). Lattice-parameter fitting (a = 8.3837 Å) supported phase stability without detectable γ-Fe_2O_3. In batch tests (C_0 = 50 mg L^{-1}, V = 100 ml, m = 0.5 g), M-CSAC achieved removals of 99.58% for Pb(II) and 96.44% for Cd(II), with Qe values of 9.958 mg/g and 9.644 mg/g, respectively. Overall, M-CSAC combines high adsorption efficiency with practical magnetic separability for water treatment.

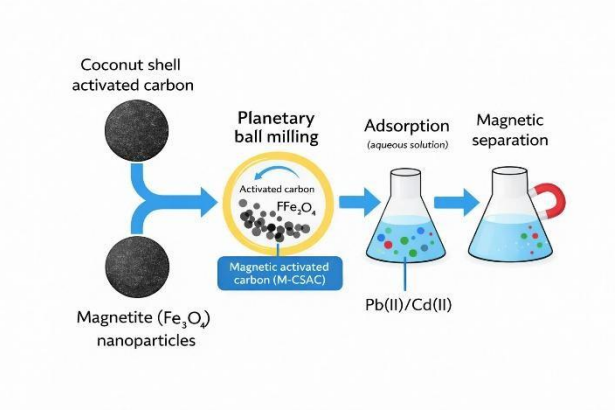

Keywords— Activated carbon, Ball milling, Cadmium(II), Lead(II), Magnetite

I. INTRODUCTION

Water pollution is an escalating global concern driven by population growth, urbanization, and industrialization. Industrial activities, including textile, ceramic, chemical, pharmaceutical, and refining sectors, generate wastewater containing toxic heavy metals and dyes. These pollutants are highly toxic, carcinogenic, and mutagenic, and can elevate Biochemical Oxygen Demand (BOD) and Chemical Oxygen Demand (COD), posing serious risks to human health and ecosystems [1], [2].

Therefore, effective approaches are required to remove heavy metal ions from aquatic environments. Adsorption is currently preferred over conventional treatment methods such as chemical precipitation, flotation, ion exchange, and membrane filtration because it is cost-effective, widely accessible, and environmentally friendly [3]. Numerous adsorbent materials, including silica gel,

[1] Departement of Chemical Engineering, Institut Teknologi Sepuluh Nopember, Sukolilo, Surabaya, 60111, Indonesia. E-mail: arm.gumilang03@gmail.com
[2] Departement of Chemical Engineering, Institut Teknologi Sepuluh Nopember, Sukolilo, Surabaya, 60111, Indonesia. Corresponding Author, E-mail: juliastuti@its.ac.id

activated alumina, activated carbon, fly ash, sugarcane bagasse, natural clay, zeolites, and various nanomaterials, have been utilized for heavy metal removal. Among these materials, activated carbon has attracted considerable interest in water treatment applications due to its high surface area, structural stability, diverse functional groups, ease of modification, and good regeneration capability [4]. Coconut shell (Cocos nucifera) is considered a promising precursor for activated carbon production. Indonesia is the world's largest coconut producer, with a total output of 17.13 million tons in 2024 according to the Food and Agriculture Organization (FAO), providing an abundant source of coconut shells that are often underutilized as organic waste. Activated carbon derived from coconut shell possesses several advantages, including a hard structure, high carbon content, and well-developed microporosity, which together provide a large active surface area for adsorption processes [5]. Previous studies have reported that coconut-shell-based activated carbon can achieve up to 98% adsorption efficiency for Pb(II) ions [6]. Moreover, it has been shown that at specific dosages, coconut shell activated carbon can remove up to 99% of Pb and 97% of Cd, highlighting its strong potential as an effective adsorbent for heavy metals [7].

Ball milling is recognized as an efficient and environmentally friendly method for the fabrication of nanomaterials, improving both the surface properties and uniformity of adsorbents [8]. S. Wang et al. demonstrated that ball-milled biochar (BC)-based composites achieved a specific surface area of 234.47 m^2/g and a maximum Pb(II) adsorption capacity of 188.15 mg/g [9]. However, BC is difficult to recycle because of its small particle size, and adsorbed Pb(II) is hard to remove under natural conditions, which can make Pb(II)-loaded BC a potential environmental hazard. Adding magnetic properties to BC allows it to be easily separated from water with minimal environmental impact compared to conventional filtration methods [10]. Conventional magnetization methods, such as co-impregnation, hydrolysis, and pyrolysis with ferric salts, are often complicated, energy-intensive, and not environmentally friendly [11]. Studies have shown that magnetic BC can be prepared by mixing BC with Fe_3O_4 using ball milling, which enhances its adsorption performance for heavy metals, antibiotics, dyes, and other pollutants while allowing easy magnetic recovery [12], [13].

In this study, magnetic activated carbon was synthesized from coconut shells with Fe_3O_4 using ball milling. The prepared magnetic adsorbents were applied for the removal of heavy metal ions, specifically Cd(II) and Pb(II), from aqueous solutions. This approach minimized the use of acids, alkalis, and organic solvents, simplified the preparation process, reduced energy consumption and production costs, and promoted the recycling and utilization of agricultural waste.

II. METHOD

A. Materials

Coconut shells were obtained from coconut processing waste in Bangunsari, Pacitan Regency, Indonesia. Lead nitrate ($Pb(NO_3)_2$), cadmium nitrate tetrahydrate ($Cd(NO_3)_2 \cdot 4H_2O$), sodium carbonate (Na_2CO_3), sodium hydroxide (NaOH) and hydrochloric acid (HCl) were purchased from ROFA Laboratory Center. Fe_3O_4 was supplied by CV. Inovasi Teknologi Nano (ITNANO), NRE Lab, Medan. All chemicals were of analytical grade and used without further purification.

B. Adsorbents Preparation

The shells, derived from coconut milk and copra oil production, were cleaned to remove impurities and residual fibers, sun-dried, and cut into smaller pieces. Carbonization was performed in a furnace at 400 °C for 1 hour to minimize oxidation and ash formation. The carbonized material was ground using a dry mill and sieved to 100 mesh to obtain uniform particle size. The carbon was washed with deionized water, filtered, and oven-dried at 110 °C for 8 hours [5]. Chemical activation was conducted by soaking the activated carbon in a 5% (w/w) Na_2CO_3 solution for 24 hours to enhance porosity and surface area. The carbon was subsequently rinsed with deionized water until neutral pH and thermally activated at 600 °C for 1 hour in a muffle furnace [14].

C. Ball-Milling Synthesis of Magnetic Activated Carbon

Magnetic modification was performed by mixing 9 g of activated carbon with 3 g of commercial Fe_3O_4 nanoparticles (99% purity) at a 3:1 mass ratio and processing in a planetary ball mill. The carbon-to-ball mass ratio was 1:50, and ball milling was conducted at 500 rpm for 6 hours with rotation direction changed after 3 hours [9], [12], [15]. This procedure produced magnetic coconut-shell-based activated carbon with improved adsorption properties and facile magnetic separation for Cd(II) and Pb(II) removal.

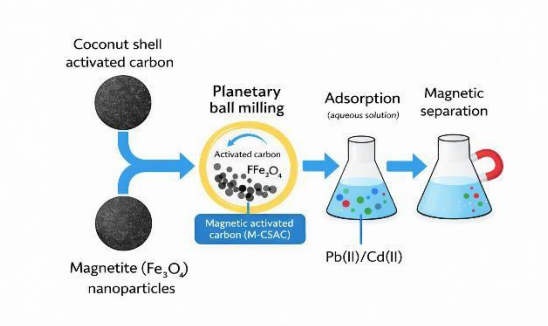

Figure 1. Schematic of magnetic coconut-shell activated carbon for Pb(II) and Cd(II) removal [12].

D. Characterization

The magnetic activated carbon was characterized to evaluate its physicochemical and structural properties prior to adsorption experiments. The surface morphology and elemental composition were analyzed using scanning electron microscopy coupled with energy-dispersive X-ray spectroscopy (SEM–EDX; ZEISS GeminiSEM, Germany), providing detailed images of the carbon surface and confirming the presence of iron (Fe). Nitrogen adsorption–desorption measurements at 77 K (BET; Nova 1200, Quantachrome, USA) were performed to determine pore properties, with specific surface area and pore size distribution calculated using the Brunauer–Emmett–Teller (BET) and Barrett–Joyner–Halenda (BJH) methods, respectively. The crystalline structure was examined using X-ray diffraction (XRD; RIGAKU MiniFlex 600, Japan) over a 2θ range of 5–80°, allowing identification of magnetite (Fe_3O_4) phases and assessment of structural changes resulting from magnetic modification and ball milling [5].

E. Pb(II) dan Cd (II) Adsorption Experiment in Aqueous Solution

Simulated wastewater containing Pb(II) and Cd(II) was prepared by dissolving $Pb(NO_3)_2$ and $Cd(NO_3)_2{\cdot}4H_2O$ in deionized water. The solution pH was adjusted using 0.1 M NaOH or HNO_3. Batch adsorption experiments were conducted to evaluate the adsorption performance of the magnetic activated carbon. For each test, 100 mg of adsorbent was added to 100 mL of metal ion solution (50 mg/l) for both Pb(II) and Cd(II)) at pH 5. The mixtures were shaken at 180 rpm at room temperature for 120 minutes. The equilibrium adsorption capacity (Q_e) and removal efficiency (η) for Pb(II) and Cd(II) were calculated using the following equations :

$$Qe = \frac{(C_0 - C_e).V}{m} \quad (1)$$

$$\eta = \frac{(C_0 - C_e)}{C_0} x\ 100\% \quad (2)$$

Here, Qe refers to the equilibrium adsorption capacity of the adsorbent (mg/g). C_0 and C_e represent the initial and equilibrium concentrations of Pb(II) or Cd(II) in the solution (mg/l). (V) is the solution volume (L), (m) is the mass of adsorbent used (g), and η denotes the percentage removal of Pb(II) or Cd(II) by the adsorbent. The preparation and application of the magnetic activated carbon are illustrated in Figure 1.

III. Results and Discussion

F. Scanning Electron Microscopy Energy-Dispersive X-Ray Spectroscopy Analysis

The microstructure and surface elemental composition of coconut shell activated carbon (CSAC) and magnetite-coconut shell activated carbon (M-CSAC) were investigated using scanning electron microscopy (SEM) coupled with energy-dispersive X-ray spectroscopy (EDX). Elemental mapping was also performed to elucidate the spatial distribution of key elements associated with heavy-metal adsorption (Pb(II) and Cd(II)).

SEM micrographs (Fig. 2) reveal clear morphological differences before and after magnetite modification. The CSAC sample (Fig. 2a, 10,000×; scale bar 1 µm) consists of relatively large and compact carbon agglomerates with a rough and irregular surface texture. After modification, the M-CSAC sample (Fig. 2b, same magnification) exhibits smaller and more fragmented agglomerates, together with finely dispersed particles distributed on the carbon surface and within interparticle spaces. These morphological changes indicate that planetary ball milling promotes the breakdown of carbon agglomerates and enhances intimate physical contact between Fe_3O_4 particles and the carbon matrix. It should be noted that the voids observed in the SEM images mainly originate from particle aggregation rather than representing intrinsic pore structures. Therefore, the pore characteristics and textural properties of the samples were quantitatively evaluated using N_2 adsorption–desorption (BET) analysis.

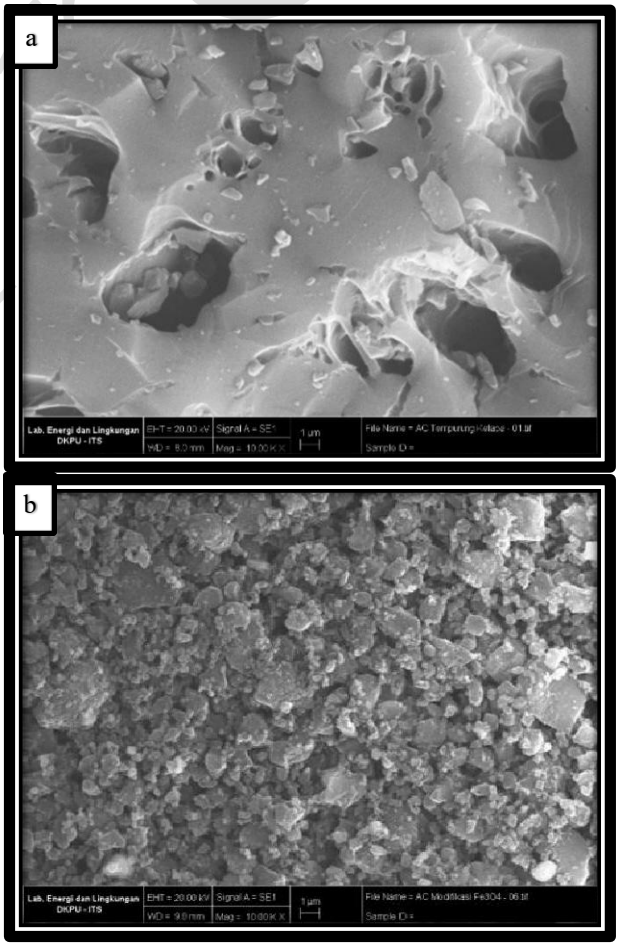

Figure 2. SEM images of (a) CSAC and (b) activate M-CSAC acquired at 10,000× (scale bar: 1 µm).

These observations are supported by EDX results (Fig. 3 and Table 1). The CSAC surface is dominated by carbon 76 wt.%, with oxygen and nitrogen contents of (13 and 9) wt.%, respectively, consistent with activated carbon enriched in oxygen and nitrogen containing surface functionalities. After modification, the M-CSAC surface composition changes markedly: the carbon fraction decreases to 62 wt.%, iron appears at 11 wt.%, oxygen increases to 26 wt.%, and nitrogen decreases to 1 wt.%.

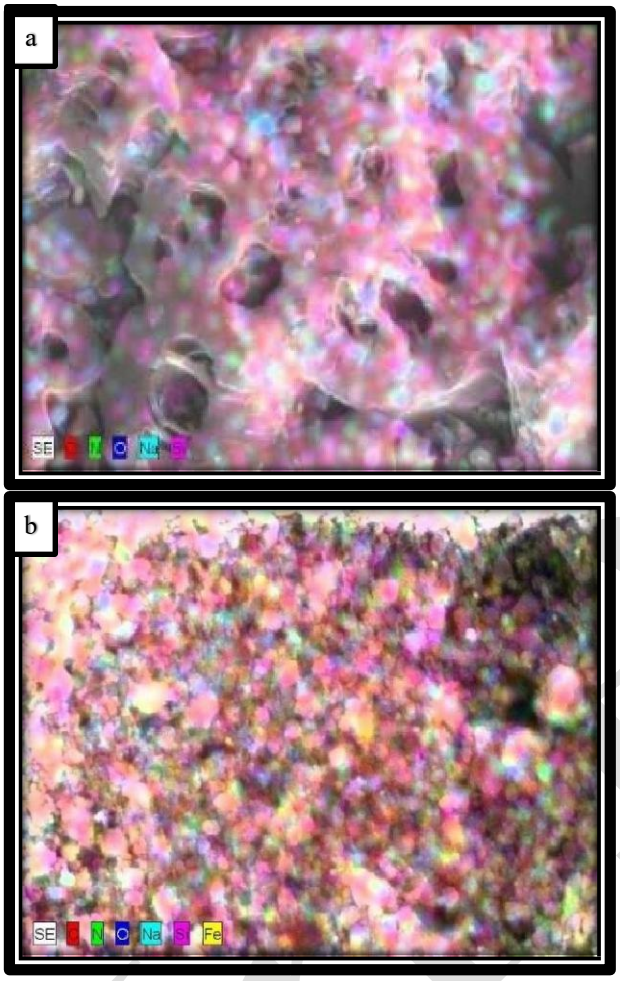

Figure 3. Surface elemental composition obtained by EDX for (a) CSAC and (b) M-CSAC.

The emergence of Fe confirms the successful incorporation and dispersion of magnetite on the carbon surface. The higher oxygen content is attributable to Fe–O bonding in the magnetite phase and potential modification of oxygenated surface groups during milling. Meanwhile, the strong decrease in nitrogen suggests partial loss or degradation of nitrogen-containing functionalities induced by the ball-milling treatment. Overall, SEM–EDX analyses demonstrate that Fe_3O_4-assisted ball milling effectively produces an activated carbon–magnetite composite with a refined surface morphology and a distinct elemental signature characterized by Fe incorporation and increased oxygen content. The formation of Fe–O-rich surface domains is expected to provide additional binding sites for Pb(II) and Cd(II), while imparting magnetic separability to the adsorbent after adsorption.

TABLE 1.
EDX ELEMENTAL COMPOSITION DATA

Material	Elemental Composition (wt. %)			
	C	O	N	Fe
CSAC	76.35	13.34	9.42	-
M-CSAC	61.63	25.95	0.99	10.73

G. Nitrogen Adsorption-Desorption Isotherms Analysis

Nitrogen adsorption–desorption isotherms were analyzed using the BET method to evaluate the specific surface area (S_{BET}) and pore-size distribution of CSAC and M-CSAC. As summarized in Table 2, magnetite modification via ball milling induced distinct changes in the textural properties. Prior to modification, CSAC exhibited an S_{BET} of 356.04 m^2/g, a total pore volume of 0.256 cm^3/g, and an average pore diameter of 2.88 nm. After magnetite incorporation, M-CSAC showed a decreased S_{BET} of 319.35 m^2/g, while the total pore volume increased to 0.316 cm^3/g and the average pore diameter widened to 3.97 nm.

TABLE 2.
SPECIFIC SURFACE AREAS AND PORE VOLUMES OF THE SAMPLE

Material	S_{BET} (m^2/g)	V_{tot} (cm^3/g)	D(nm)
CSAC	356.044	0.256	2.88
M-CSAC	319.345	0.3166	3.97

S_{BET}: BET surface area; V_{tot}: total pore volume; D: Average pore diameter

The simultaneous decrease in S_{BET} and increase in total pore volume and average pore diameter suggests that Fe_3O_4 addition through ball milling not only introduces a magnetic phase but also alters the pore architecture of the activated carbon. This behavior implies that Fe_3O_4 nanoparticles are well dispersed and physically anchored within the carbon matrix, leading to partial blocking or filling of micropores and, concurrently, the widening and/or coalescence of smaller pores into mesopores.

The adsorption–desorption isotherms of both materials (Fig. 4a and 5a) can be classified as type IV with a pronounced hysteresis loop at intermediate-to-high relative pressures (P/P_0), indicating the presence of mesoporous structures. The larger N_2 uptake of M-CSAC compared with CSAC, particularly at high P/P_0, is consistent with the higher total pore volume of the

modified composite. Furthermore, BJH pore-size distribution plots (Fig. 4b and 5b) show that CSAC is dominated by pores centered at 3 nm with a relatively narrow distribution, whereas M-CSAC exhibits a peak shifted toward 3–4 nm and a broader distribution extending to larger pore sizes.

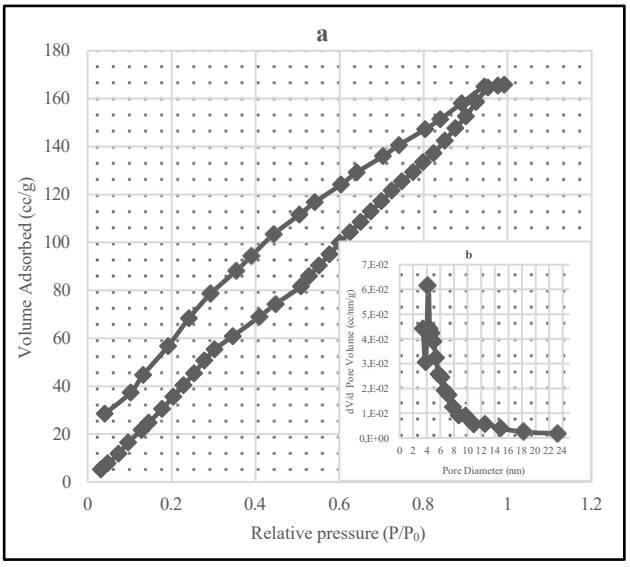

Figure 4. Nitrogen adsorption-desorption isotherms (a) and pore size distribution curves (b) of CSAC

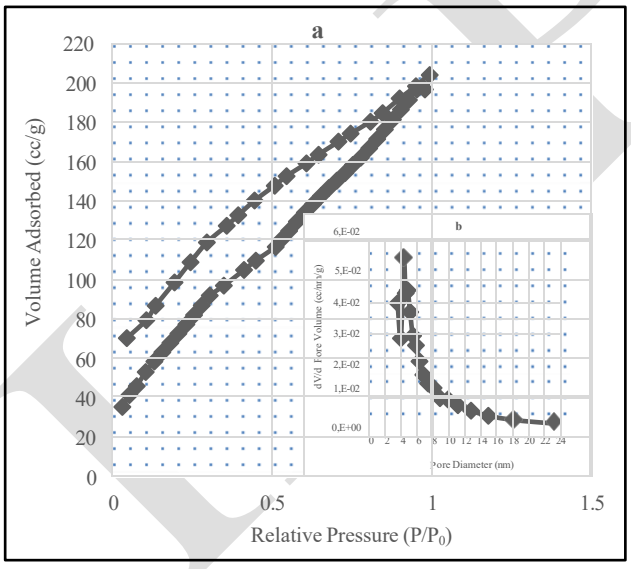

Figure 5. Nitrogen adsorption-desorption isotherms (a) and pore size distribution curves (b) of M-CSAC.

H. X-ray Diffraction Analysis

In this study, X-ray diffraction (XRD) was employed to verify that the ball-milling synthesis of M-CSAC did not induce phase transformation of magnetite (Fe_3O_4) into maghemite (γ-Fe_2O_3). This verification is essential because mechanical milling can generate high-impact energy, localized heating, and increased exposure to oxygen, all of which may accelerate the oxidation of Fe^{2+} to Fe^{3+} [16]. The XRD pattern of M-CSAC (Fig. 6) displays distinct diffraction peaks characteristic of magnetite (Fe_3O_4) at 2θ = 30.24°, 35.40°, 43.18°, 57.00°, and 62.50°.

These reflections can be indexed to the (220), (311), (400), (511), and (440) planes, respectively, in good agreement with the standard magnetite reference (JCPDS PDF 00-019-0629). The close match suggests that the formed magnetic phase is predominantly polycrystalline magnetite (Fe_3O_4) [17], [18]. Distinguishing magnetite (Fe_3O_4) from maghemite (γ-Fe_2O_3) by XRD is inherently challenging because both phases share a spinel structure and exhibit very similar lattice parameters. Maghemite has been reported to present additional weak reflections at approximately 2θ = 23.77° and 26.10°, assigned to the (210) and (211) planes, which may serve as diagnostic features for phase discrimination [19].

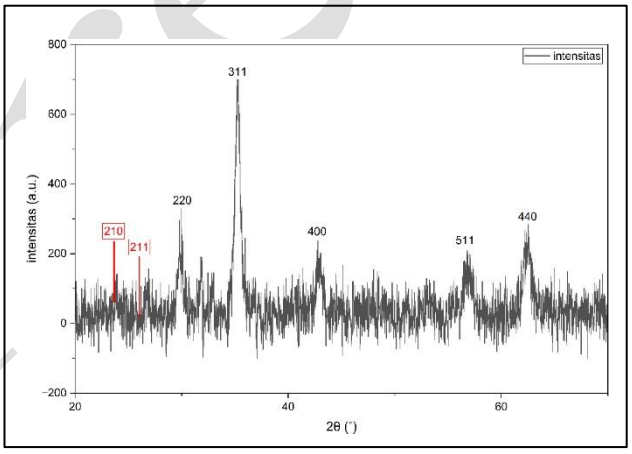

Figure 6. XRD pattern of M-CSAC.

In Fig. 6, the red markers indicating these maghemite positions do not show discernible diffraction peaks, supporting within the detection limit of XRD the absence of γ-Fe_2O_3 in the prepared sample. Nevertheless, it should be noted that the (210) and (211) reflections of maghemite can be very low in intensity. Therefore, the lack of these peaks alone should not be considered the sole criterion for definitive confirmation of maghemite absence.

Table 3 shows that the main diffraction peak positions of M-CSAC sample in this study closely match those of the Fe_3O_4 reference pattern (JCPDS 19-0629) and are slightly shifted relative to the γ-Fe_2O_3 reference (JCPDS 39-1346). This further indicates that the obtained diffraction pattern is more consistent with the magnetite phase than with maghemite. This interpretation is supported by the lattice parameter derived from profile fitting using "Match!" for the same sample, yielding (a = 8.3837 Å). The obtained

value is closer to the reported lattice parameter of Fe_3O_4 JCPDS (a = 8.396 Å) than that of γ-Fe_2O_3 (a = 8.3515 Å), confirming that magnetite (Fe_3O_4) is the dominant crystalline phase in the activated carbon–magnetite composite.

TABLE 3.
MAIN XRD PEAK POSITIONS (2Θ, Cu Ka) OF M-CSAC SAMPLE COMPARED WITH JCPDS REFERENCE PATTERNS.

hkl	M-CSAC *in this study*	Fe_3O_4 (JCPDS 19-0629)	γ-Fe_2O_3 (JCPDS 39-1346)
(220)	30.24°	30.095°	30.241°
(311)	35.40°	35.423°	35.631°
(400)	43.18°	43.053°	43.285°
(511)	57.00°	57.033°	57.277°
(220)	62.50°	62.516°	62.927°

I. *Pb(II) Adsorption Experiments In Simulated Wastewater*

After physicochemical characterization, M-CSAC was evaluated for its adsorption performance toward aqueous solutions containing Pb(II) and Cd(II). Overall, the results in Fig. 7 demonstrate that M-CSAC exhibits excellent adsorption capability for both metal ions. Under identical operating conditions (C_0 = 50 mg/l, V = 100 mL, m = 0.5 g), M-CSAC achieved very high removal efficiencies for Pb(II) and Cd(II). The equilibrium uptake Qe values approaching 10 mg/g for both systems indicate that nearly all of the metal ions initially present in solution were removed by 0.5 g of adsorbent. The slightly higher removal efficiency and adsorption capacity for Pb(II) than for Cd(II) suggests a stronger affinity of the M-CSAC surface toward Pb(II), which may be attributed to differences in ionic characteristics and the specific interactions of Pb(II) and Cd(II) with functional groups on the modified activated carbon surface.

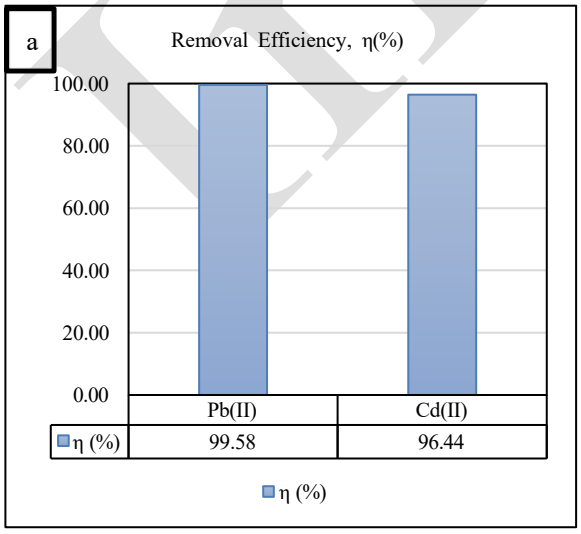

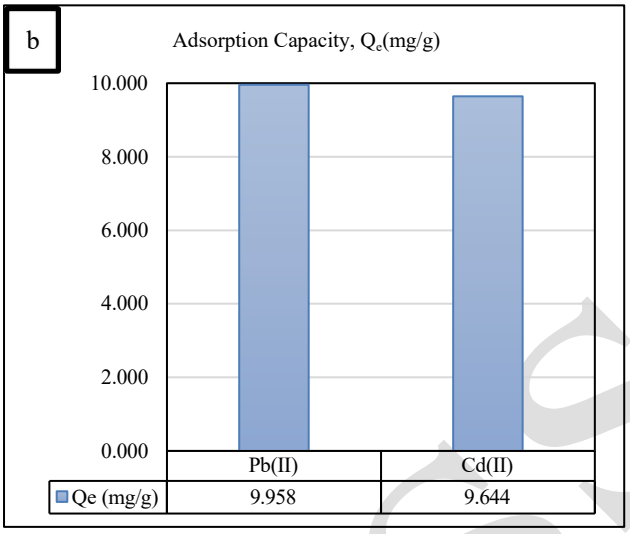

Figure 7. Removal efficiency, η (a) and adsorption capacity, Qe (b) for Pb(II) and Cd(II) ions.

The crystallinity of the Fe_3O_4 phase primarily affects the structural stability and surface reactivity of the composite rather than directly governing its adsorption capacity. Previous studies have shown that moderately crystalline or nanocrystalline iron oxides possess a higher density of surface hydroxyl groups (Fe–OH), which serve as active sites for metal ion binding, whereas excessive crystallinity may reduce surface reactivity [9]. The lower adsorption performance observed for Cd(II) compared to Pb(II) is consistent with established adsorption theory, as Cd(II) exhibits higher hydration energy and weaker surface complexation. In contrast, Pb(II) forms stronger inner-sphere complexes with oxygen-containing functional groups and iron oxide surfaces [20]. This difference in adsorption behavior can also be explained by Pearson's Hard Soft Acid Base (HSAB) theory, where Pb(II), being a softer Lewis acid than Cd(II), shows stronger affinity toward oxygen-donor functional groups on the adsorbent surface, resulting in more stable surface complexes and higher adsorption efficiency [21].

J. *Reusability Of Magnetic Adsorbent*

Regeneration is a critical consideration for assessing the practicality and cost-effectiveness of an adsorbent [22]. Desorption, which proceeds as the reverse of metal-ion uptake, is essential for evaluating adsorbent reusability [23]. Magnetic adsorbents have the advantage of making recycling more convenient. The regeneration mechanism of M-CSAC is based on HCl elution, where the acidic medium facilitates the release of Pb(II) and Cd(II) species from the adsorption sites and regenerates the surface for reuse.

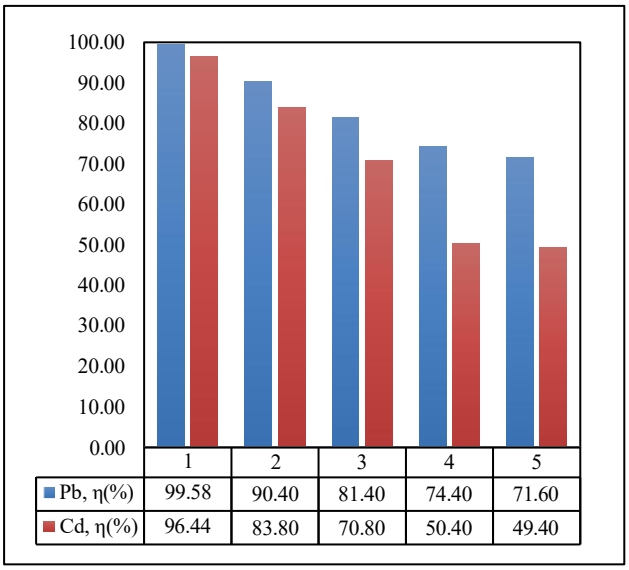

	1	2	3	4	5
Pb, η(%)	99.58	90.40	81.40	74.40	71.60
Cd, η(%)	96.44	83.80	70.80	50.40	49.40

Figure 8. Regeneration performance of magnetic adsorbents.

As shown in Fig. 8, after the first adsorption magnetic recovery desorption cycle, the removal efficiencies of AC–M for Pb(II) and Cd(II) at an initial concentration of 50 mg/l were 99.8% and 96.44%, respectively. After 5 cycles, the removal efficiencies decreased by 27.98% Pb(II) and 47.04% Cd(II), indicating that a minor fraction of metal ions was irreversibly retained on the adsorbent surface. Nevertheless, M-CSAC preserved satisfactory removal performance after repeated cycles, demonstrating its potential as an efficient and regenerable adsorbent for heavy-metal remediation.

IV. CONCLUSION

Magnetite-modified coconut-shell activated carbon (M-CSAC) was successfully prepared via Fe_3O_4 assisted ball milling, yielding a magnetically recoverable adsorbent for Pb(II) and Cd(II) removal. Structural and surface analyses confirmed effective magnetite incorporation, as indicated by the presence of Fe in EDX and Fe_3O_4 reflections in XRD, with no detectable γ-Fe_2O_3 within the XRD detection limit. Textural characterization showed that magnetization slightly reduced the specific surface area but increased total pore volume and enlarged the average pore diameter, suggesting partial micropore blocking accompanied by pore widening toward mesoporosity. Under batch conditions, M-CSAC achieved high removals of Pb(II) 99.58% and Cd(II) 96.44%, with equilibrium capacities close to 10 mg/g. These results demonstrate that mechanochemical magnetization can enhance the practical applicability of biomass derived activated carbon by enabling magnetic separation while maintaining excellent adsorption performance. Future work is recommended to evaluate adsorbent reusability, competitive ion effects, and performance in real wastewater matrices to further support scale-up and application.

V. ACKNOWLEDGEMENTS

The authors sincerely thank the Directorate of Research and Community Service at Sepuluh Nopember Institute of Technology (ITS), Surabaya, Indonesia, for their valuable assistance and the facilities that contributed to the successful completion of this research.

REFERENCES

[1] M. Raninga, A. Mudgal, V. K. Patel, J. Patel, and M. Kumar Sinha, "Modification of activated carbon-based adsorbent for removal of industrial dyes and heavy metals: A review," in *Materials Today: Proceedings*, Elsevier Ltd, Jan. 2023, pp. 286–294. doi: 10.1016/j.matpr.2022.11.358.

[2] S. Jha, R. Gaur, S. Shahabuddin, and I. Tyagi, "Biochar as Sustainable Alternative and Green Adsorbent for the Remediation of Noxious Pollutants: A Comprehensive Review," Feb. 01, 2023, *MDPI*. doi: 10.3390/toxics11020117.

[3] Renu and T. Sithole, "A review on regeneration of adsorbent and recovery of metals: Adsorbent disposal and regeneration mechanism," Oct. 01, 2024, *Elsevier B.V.* doi: 10.1016/j.sajce.2024.07.006.

[4] L. Jaber *et al.*, "Adsorptive Removal of Lead and Chromate Ions from Water by Using Iron-Doped Granular Activated Carbon Obtained from Coconut Shells," *Sustainability (Switzerland)*, vol. 14, no. 17, Sep. 2022, doi: 10.3390/su141710877.

[5] P. Baskaran and M. Abraham, "Adsorption of cadmium (Cd) and lead (Pb) using powdered activated carbon derived from Cocos Nucifera waste: A kinetics and equilibrium study for long-term sustainability," *Sustainable Energy Technologies and Assessments*, vol. 53, Oct. 2022, doi: 10.1016/j.seta.2022.102709.

[6] J. Chen *et al.*, "Modified coconut shell biochars (MCSBCs): Fabrication and their adsorptions for Pb(II)," *Heliyon*, vol. 10, no. 11, Jun. 2024, doi: 10.1016/j.heliyon.2024.e32422.

[7] H. Qin, X. Shao, H. Shaghaleh, W. Gao, and Y. A. Hamoud, "Adsorption of Pb2+ and Cd2+ in Agricultural Water by Potassium Permanganate and Nitric Acid-Modified Coconut Shell Biochar," *Agronomy*, vol. 13, no. 7, Jul. 2023, doi: 10.3390/agronomy13071813.

[8] G. Gorrasi and A. Sorrentino, "Mechanical milling as a technology to produce structural and functional bio-nanocomposites," *Green Chem.*, vol. 17, no. 5, pp. 2610–2625, 2015, doi: 10.1039/C5GC00029G.

[9] S. Wang *et al.*, "Halloysite and coconut shell biochar magnetic composites for the sorption of Pb(II) in wastewater: Synthesis, characterization and mechanism investigation," *J. Environ. Chem. Eng.*, vol. 9, no. 6, Dec. 2021, doi: 10.1016/j.jece.2021.106865.

[10] S. Zhang, Y. Ji, J. Dang, J. Zhao, and S. Chen, "Magnetic apple pomace biochar: Simple preparation, characterization, and application for enriching Ag(I) in effluents," *Science of The Total Environment*, vol. 668, pp. 115–123, Jun. 2019, doi: 10.1016/J.SCITOTENV.2019.02.318.

[11] K. R. Thines, E. C. Abdullah, N. M. Mubarak, and M. Ruthiraan, "Synthesis of magnetic biochar from agricultural waste biomass to enhancing route for waste water and polymer application: A review," *Renewable and Sustainable Energy Reviews*, vol. 67, pp. 257–276, Jan. 2017, doi: 10.1016/J.RSER.2016.09.057.

[12] T. Ai, X. Jiang, Q. Liu, L. Lv, and H. Wu, "Daptomycin adsorption on magnetic ultra-fine wood-based biochars from water: Kinetics, isotherms, and mechanism studies," *Bioresour. Technol.*, vol. 273, pp. 8–15, Feb. 2019, doi: 10.1016/J.BIORTECH.2018.10.039.

[13] D. Shan *et al.*, "Preparation of ultrafine magnetic biochar and activated carbon for pharmaceutical adsorption and subsequent degradation by ball milling," *J. Hazard. Mater.*, vol. 305, pp. 156–163, Mar. 2016, doi: 10.1016/J.JHAZMAT.2015.11.047.

[14] E. Suryani *et al.*, "Chimica et Natura Acta Sintesis Karbon Aktif Magnetik dari Tempurung Kelapa menggunakan Aktivator Soda Kue dengan Variasi Perbandingan Massa Karbon Aktif dan Oksida Besi," vol. 12, no. 1, pp. 19–27, 2024, doi: 10.24198/cna.v12.n1.42382.

[15] D. Shan *et al.*, "Preparation of ultrafine magnetic biochar and activated carbon for pharmaceutical adsorption and subsequent degradation by ball milling," *J. Hazard. Mater.*, vol. 305, pp. 156–163, Mar. 2016, doi: 10.1016/j.jhazmat.2015.11.047.

[16] E. Madiha *et al.*, "Structural, Electromagnetic and Microwave Properties of Magnetite Extracted from Mill Scale Waste via Conventional Ball Milling and Mechanical Alloying Techniques," *Materials*, vol. 14, Nov. 2021, doi: 10.3390/ma14227075.

[17] M. I. Dar and S. A. Shivashankar, "Single crystalline magnetite, maghemite, and hematite nanoparticles with rich coercivity," *RSC Adv.*, vol. 4, pp. 4105–4113, 2014, [Online]. Available: https://api.semanticscholar.org/CorpusID:97686277

[18] C. Wroblewski, T. Volford, B. Martos, J. Samoluk, and P. Martos, "High Yield Synthesis and Application of Magnetite Nanoparticles (Fe3O4)," *Magnetochemistry*, vol. 6, no. 2, 2020, doi: 10.3390/magnetochemistry6020022.

[19] W. Kim *et al.*, "A new method for the identification and quantification of magnetite–maghemite mixture using conventional X-ray diffraction technique," *Talanta*, vol. 94, pp. 348–352, May 2012, doi: 10.1016/J.TALANTA.2012.03.001.

[20] S. Babel and T. A. Kurniawan, "Low-cost adsorbents for heavy metals uptake from contaminated water: a review," *J. Hazard. Mater.*, vol. 97, no. 1–3, pp. 219–243, Feb. 2003, doi: 10.1016/S0304-3894(02)00263-7.

[21] A. Bashir, T. Manzoor, L. A. Malik, A. Qureashi, and A. H. Pandith, "Enhanced and Selective Adsorption of Zn(II), Pb(II), Cd(II), and Hg(II) Ions by a Dumbbell- and Flower-Shaped Potato Starch Phosphate Polymer: A Combined Experimental and DFT Calculation Study," *ACS Omega*, vol. 5, no. 10, pp. 4853–4867, Mar. 2020, doi: 10.1021/acsomega.9b03607.

[22] R. Sinha, R. Kumar, P. Sharma, N. Kant, J. Shang, and T. M. Aminabhavi, "Removal of hexavalent chromium via biochar-based adsorbents: State-of-the-art, challenges, and future perspectives," *J. Environ. Manage.*, vol. 317, p. 115356, Sep. 2022, doi: 10.1016/J.JENVMAN.2022.115356.

[23] Poonam, S. K. Bharti, and N. Kumar, "Kinetic study of lead (Pb2+) removal from battery manufacturing wastewater using bagasse biochar as biosorbent," *Appl. Water Sci.*, vol. 8, no. 4, p. 119, 2018, doi: 10.1007/s13201-018-0765-z.